Contents lists available at ScienceDirect

Food and Bioproducts Processing

journal homepage: www.elsevier.com/locate/fbp

Evaluating the displacement field of paperboard packages subjected to compression loading using digital image correlation (DIC)

Tobi Fadiji[a,b], Corné J. Coetzee[a], Umezuruike Linus Opara[b,*]

[a] Department of Mechanical and Mechatronics Engineering, Faculty of Engineering, Stellenbosch University, South Africa

[b] Postharvest Technology Research Laboratory, South African Research Chair in Postharvest Technology, Department of Horticultural Sciences, Faculty of AgriSciences, Stellenbosch University, South Africa

ARTICLE INFO

Article history:
Received 17 March 2020
Received in revised form 26 May 2020
Accepted 9 June 2020
Available online 19 June 2020

Keywords:
Digital image correlation (DIC)
Displacement
Strain
Corrugated paperboard packages
Compression test
Package design

ABSTRACT

Digital image correlation (DIC) is a full-field non-contact optical technique for measuring displacements in experimental testing based on correlating several digital images taken during the test, particularly images before and after deformation. Application of DIC cuts across several fields, particularly in experimental solid mechanics; however, its potential application to paperboard packaging has not been fully explored. To preserve fresh horticultural produce during postharvest handling, it is crucial to understand how the packages deform under mechanical loading. In this study, 3D digital image correlation with two cameras and stereovision was used to determine the full-field displacement of corrugated paperboard packaging subjected to compression loading. Strain fields were derived from the displacement fields. Results obtained from the displacement fields showed the initiation and development of the buckling behaviour of the carton panels. The displacement was observed to be largely heterogeneous. The displacement field in the horizontal direction was smaller compared to that of vertical and out-of-plane directions. In addition, the strain variation increased as load increased, which could be a precursor to material failure. The technique proved to be efficient in providing relevant information on the displacement and strain fields at the surface panels of corrugated paperboard packages used for handling horticultural produce. In addition, it offers prospects for improved mechanical design of fresh produce packaging.

1. Introduction

Paper as a packaging material has been widely utilised for various products such as food, horticultural produce (fruit and vegetables, etc.), medicine, clothing, electronics, among others (Zhou et al., 2013). This packaging material is widely adopted for manufacturing ventilated cartons for handling different produce in the fresh fruit industry (Fadiji et al., 2016a), because it belongs to a group of flexible materials, low in cost and has an excellent lightweight performance, i.e. its low weight-to-strength ratio and high stiffness-to-weight ratio (Flatscher et al., 2011). Ventilated paperboard package in fresh fruit industries is commonly used due to its ability to promote rapid and efficient cooling while providing sufficient mechanical strength. However, during postharvest handling, the cartons are exposed to different mechanical loadings which could be detrimental to its mechanical integrity (Fadiji et al., 2016b). An important quality index for the cartons is

* Corresponding author.
E-mail addresses: opara@sun.ac.za, umunam@yahoo.co.uk (U.L. Opara).
https://doi.org/10.1016/j.fbp.2020.06.008
0960-3085/

its compression strength which is referred to as the maximum load and deformation of the damaged cartons under uniform dynamic pressure exerted by the compression testing machine (Gong et al., 2020). Compression strength values of packages usually include the deflection (a measure of how much a carton is compressed) at failure or at the end of a specific load application.

When the cartons are subjected to vertical load from top to bottom, the load is resisted by the side panels of the cartons, and continuous application of the load leads to instability in the side panels and eventually collapse of the cartons. The phenomenon of the structural loss is known as buckling (Gong et al., 2020). Pathare and Opara (2014) pointed out that the most common failure mode for a carton loaded in top-to-bottom compression is post-buckling deflection of its side panels, followed by a biaxial compressive failure of the board in the highly stressed regions of the carton. The theoretical, experimental, and numerical analyses of the deformation and compressive strength of paperboard cartons have been reported by different researchers and summarised in the review by Fadiji et al. (2018). The study by Fadiji et al. (2019a) used validated finite element analysis (FEA) to evaluate the performance of ventilated packages by considering the functionality of package vent holes and geometrical nonlinearities. The FEA model accurately predicted the compression strength and deformation of the packages. Another study by Gong et al. (2020) used experimental and numerical techniques to analyse the deformation and compressive capacity of cartons under the indentation condition of different shapes.

While these techniques are used successfully to evaluate the deformation of cartons, Pan (2018) reported the viability and predominance of digital image correlation (DIC) in the measurement of surface deformation, particularly in solid mechanics. DIC is a non-interferometric optical technique which compares the grey intensity changes on the surface of an object before and after deformation (Pan and Li, 2011). It has very distinct advantages of simple experimental set-up, minimum requirements on the experimental environment without the need for laser source and a wide range of its application. Even though the DIC technique has minimal requirements when it comes to the experimental environment, it is not trouble-free. With the technique based on matching images or patterns, for instance, before and after deformation, it implies that measurements rely strongly on the quality of the acquired images.

Strain measurement and the elastic properties of materials like silicon, steel, polycrystalline, and brittle materials have been determined using DIC (Godara et al., 2009; Chasiotis and Knauss, 2002). Although there is a limited application of DIC on paper and paperboards, there are some evidences that the mechanical behaviour, when subjected to various loads, can be determined using this technique for displacement and strain measurements (Viguié and Dumont, 2013). For example, the local grammage and local strain were reported by Wong et al. (1996) to be inversely proportional in uncalendared paper sheets using DIC. In the study by Thorpe and Choi (1992), the authors measured the strains on the surface of a box panel subjected to compression with a two-dimensional (2D) DIC by considering both the convex and concave buckling modes. The information obtained by the authors was incomplete and particularly not sufficient when dealing with buckling problems because the contribution of the out-of-plane displacement to the strain components was not considered. Allansson and Svärd (2001) measured the displacement field of a board panel under compression with a supporting frame in the out of plane direction using a digital speckle photography technique. The study by Considine et al. (2005) used direct observation to evaluate the local deformation of paperboard and hand sheets. The authors used DIC to capture and analyse images under increasing tension and found the variation in strain to increase with an increase in load. The strain became more erratic near failure, indicating many local failures.

A great improvement in the DIC technique is in its capability to measure a three-dimensional (3D) displacement field and surface strain field of any 3D object (Viguié et al., 2011). However, the use of DIC to measure the displacement field of ventilated packages subjected to mechanical loads has not yet been reported in detail. A recent study by Kueh et al. (2019) examined the contributions to displacement of panels of compressed boxes using 3D DIC, however, the study did not consider the influence of vent holes. Vent hole designs have been reported to affect the overall mechanical integrity of cartons (Fadiji et al., 2016b). It is therefore important to know the deformation pattern and localised straining of the carton particularly as affected by geometrical configurations such as the vent holes. Thus, this study aimed to deepen the knowledge of the displacement field of corrugated paperboard packages under compression loading, by considering the influence of different geometrical configurations of vents. This present study follows up on the studies by Fadiji et al. (2019a) and Berry et al. (2017). The former investigated the structural integrity using validated finite element analysis (FEA) simulations of similar packages while the latter used a multi-parameter strategy with computational fluid dynamics (CFD) simulations to evaluate airflow characteristics and cooling properties of similar packages. These studies provide valuable baseline data to guide further studies on comprehensively understanding the effects of package design on produce quality and shelf life.

2. Basic principles of digital image correlation (DIC)

The concept of using DIC for determining surface deformation was proposed at the beginning of the 1980s by a group of researchers at the University of Carolina, when it was applied to solid mechanics (Pan et al., 2009). Its development over the years has made DIC technique powerful and popular in areas such as fracture mechanics, full-field motion, high-temperature deformation measurements, biomaterials, inverse stress analysis and wood products etc. (Pan and Li, 2011). In recent years, the technique of DIC has been applied to deformation measurements of images acquired from X-ray microtomography, scanning electron microscopy (SEM) and atomic force microscopy (AFM).

DIC is an application based on the comparison of two images acquired at different states, one before deformation and the other one after deformation (Hung and Voloshin, 2003). These images are referred to as reference and deformed images, respectively. In another definition by Pan et al. (2010), the author defined DIC as non-contact, full-field optical metrology used to measure deformation accurately, which could be two-dimensional (2D) or three-dimensional (3D) and shape obtained from digital images of the test object surface, which are recorded at different configurations. The basic principle of digital image correlation involves tracking or matching of the same points (pixels) between the image captured before deformation and a series of deformed images captured after

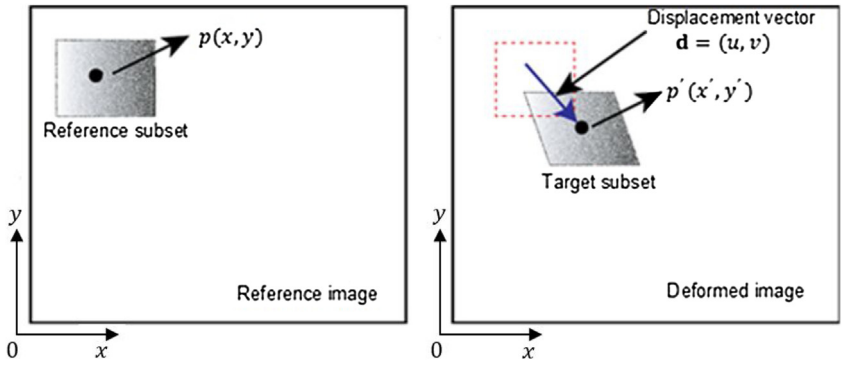

Fig. 1 – Schematic diagram of the reference subset (left) and deformed subset (right) before and after deformation, respectively.

deformation as shown in Fig. 1 (Tekieli et al., 2017). To be able to compute the displacement at point p, a square reference subset of $(2M+1) \times (2M+1)$ pixels, centralised at $p(x,y)$ from the reference image is chosen and used as a tracking means of its corresponding position in the deformed image (Pan et al., 2009).

The test samples must be covered with a random speckle pattern, serving as a deformation information carrier (Pan et al., 2012). These pictures are converted to greyscale from a RGB colour model and treated as a matrix. Each matrix element equals a pixel that represents a specific point on the sample surface, with its value based on its intensity from black to white (Tekieli et al., 2017).

To determine the displacement, a ROI (Region of Interest) which is a computational grid is defined on the sample's surface. The position of the speckles in the ROI taken before and after deformation is correlated. Based on the correlation criteria used, the displacement field can be computed. As outlined by Tang et al. (2012) and Pan et al. (2010), to evaluate the correspondence between the reference and deformed subsets, the cross-correlation (CC) criterion or the sum of squared difference (SSD) criterion can be used.

3. Materials and methods

3.1. *Packaging materials and their properties*

Three package types were used in this study: unvented Control package and two ventilated corrugated paperboard packages (VCP) referred to as the Standard and the Multi vent designs. The packages were fabricated using a corrugated paperboard die cutter and then assembled and glued. The Standard vent design is specifically used for handling pome fruit in international trade from South Africa (Berry et al., 2017) while the Multi vent design was proposed as an alternative to the Standard vent design (Fadiji et al., 2019a, b). The packages are regular slotted cartons, which consist of inner and outer boxes, made with single-wall corrugated paperboard. Both Standard and Multi vent designs have oblong-shaped vent holes oriented vertically on the long and short sides of the packages. The total vent area of both the VCP packages was 4%. For all the package types, the paperboard grammage combination was 250K/175B/250K for the outer carton and 250K/175C/250K for the inner carton. The numerical values indicate the paperboard combinations (fluting and liners) grammages ($g\,m^{-2}$). K indicates Kraft linerboards while B and C indicate the fluting profile of the paperboard. The thickness of the liners was 0.349 ± 0.002 mm while the thickness of the flute was 0.249 ± 0.002 mm. The outer dimensions of the packages are 500 mm × 333 mm × 270 mm. Fig. 2 shows the geometry of the control package, Standard vent and Multi vent designs while Fig. 3 shows the dimensions of the Standard and Multi vent designs.

3.2. *Package compression test*

The Lansmont compression tester (Lansmont Corporation, Monterey CA, USA), with a maximum force of 22.2 kN was used to determine the compressive strength of the packages. The test was done following the recommendations of the ASTM D642 standard (ASTM, 2010). A preload of 222 N was applied to remove the initial transient effects, prior to obtaining the compression strength values. The fixed platen mode of the compression tester was used to conduct the compression test at a continuous speed of 12.7 ± 2.5 mm min^{-1} until failure was observed. Before the compression test, the packages were preconditioned at $30 \pm 1\,^{\circ}C$ and RH of 20–30% for 24 h and then conditioned at $23 \pm 1\,^{\circ}C$ and 50% RH for 24 h according to ASTM D4332 standard (ASTM, 2006). Five replicates for the different package designs were used for the compression test. During the compression test, as the load is applied progressively, a level of the load is reached where the panels of the package become unstable and bend laterally. This unstable behaviour causes the central region of the panel to decrease significantly in its ability to withstand a further increase in load. The compressive load or the force applied by the box tester and crosshead displacement were recorded continuously until collapse occurred (i.e. failure).

3.3. *DIC technique for displacement field of the package*

Fig. 4 shows a schematic experimental set-up of a 3D DIC method used in this study. The DIC full-field measurements were made during the compression test with the LaVision® camera and software (LaVision Inc., Ypsilanti, MI, USA). The LaVision® 3D system consists: two charge-coupled device (CCD) cameras with a 5-megapixel resolution, with the lenses having a focal length of 35 mm, LED light sources for illumination, and a computer with installed DaVis DIC software. The DIC system can measure in-plane and out-of-plane deformation. For the package preparation, a speckle pattern consisting of black dots was randomly applied on the white surface of the package (Fig. 5). The accuracy of the results may be affected by the size of the dots in the speckle pattern (Tekieli et al., 2017), hence a suitable balance was ensured based on the

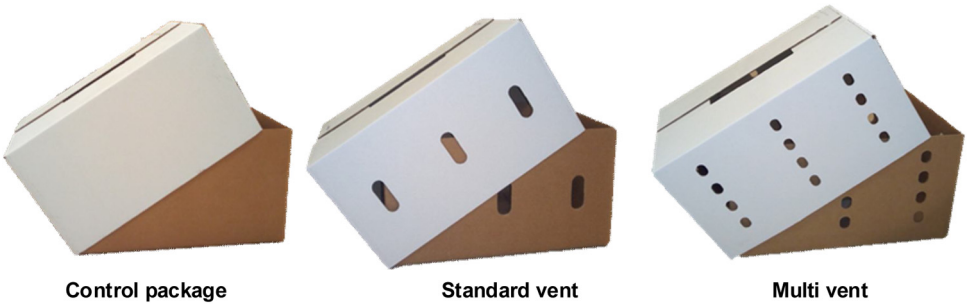

Fig. 2 – Geometry of the different packages used.

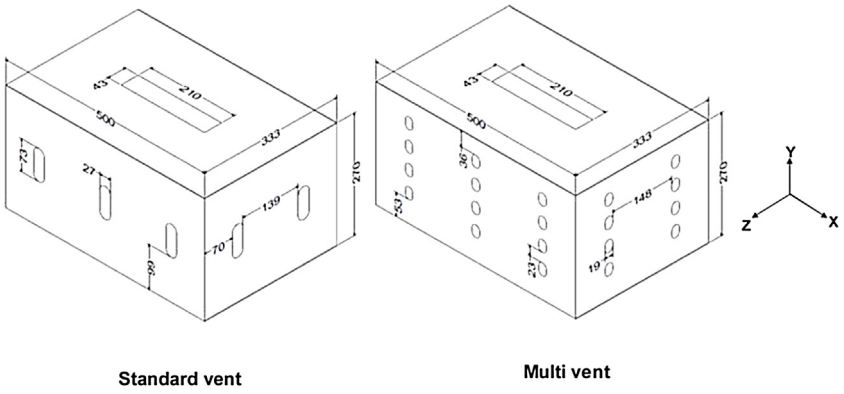

Fig. 3 – Geometry showing the dimensions (in mm) of the standard and multi vent designs.

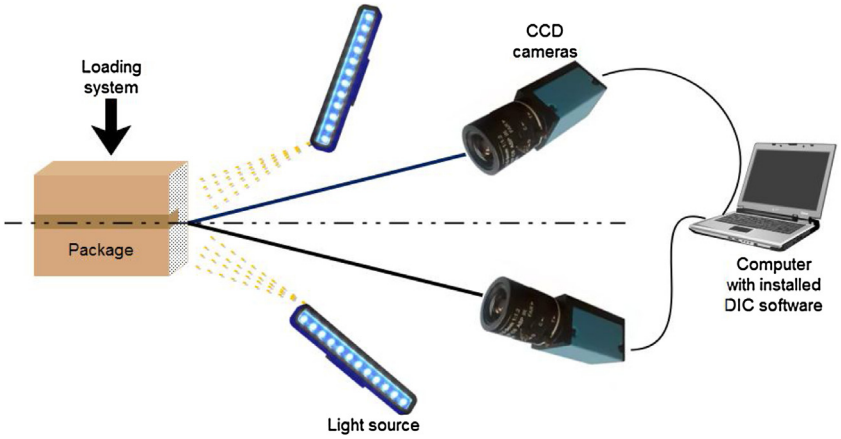

Fig. 4 – Schematic diagram of 3D digital image correlation (DIC) setup.

experimental setup. For this study, the black dots were larger than three pixels to avoid poor correlation due to noise from the test. The test was done within a short time after the spray painting to avoid aged speckle patterns, which could cause the paint to flake off leading to inaccurate measurements.

The concept of simple binocular vision is used in 3D image correlation and it applies a detailed calibration procedure to model the cameras (Kolanu et al., 2016). An accurate approximation of the same specimen location can be determined for the 3D position with the sensor plane locations in both views for the same specimen point, once the two cameras are calibrated. The synchronisation of the image acquisition process is possible after the calibration to allow the two cameras to capture images simultaneously during the test. To assign the physical dimensions to the images, calibration of the image is required. The calibration plates on the ROI are shown in Fig. 5. Using the co-ordinate system of the calibration plate, a co-ordinate system was defined. The side of the package that was observed during the compression was half of the lengthwise side of the package.

As the objective of this study is to understand the displacement field of paperboard packages under compression loading, the images were acquired during the compression test at a frequency of 2 Hz. The exposure time for all the imaging was 3000 μs. Also, the LED light was set to flash at each time an image is taken, as this helps to prevent the influence of temperature increase, which can adversely affect the measurements when using continuous illumination. The method of subset matching from the acquired images was used to determine the displacements. In this study, square pixel × pixel subsets sizes were used in the analyses. The

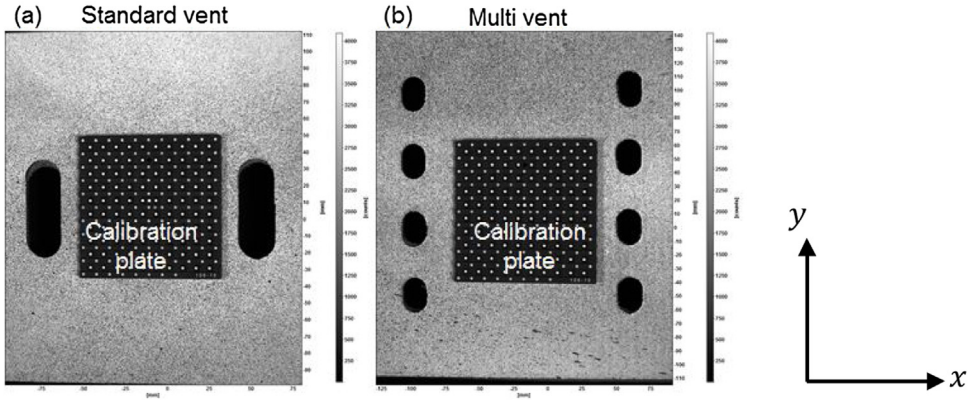

Fig. 5 – Typical speckle pattern used in the measurement: (a) standard vent and (b) multi vent. The region of interest is also shown.

subset used was 121 × 121 pixel, and the correlation was performed with a step size of 8 pixels. The small step size used was chosen to ensure a dense displacement field. To match subsets from the reference image to the deformed image, the ZNSSD correlation method was employed (Huchzermeyer, 2017). The correlation was done using the DaVis DIC software, after which the displacement fields were exported from and imported into Matlab for further processing. Strain in LaVision® is calculated through central differencing, which is the relative displacement over a gauge length. A 6th order spline interpolation scheme, which is the accurate setting in LaVision® was used for determining sub-pixel coordinates. This interpolation scheme results in less susceptibility to pixel locking.

4. Results and discussion

4.1. *Package compression strength and displacement*

A typical load-displacement curve for all the package designs is shown in Fig. 6. From the curves, a low stiffness was observed at the initiation of compression which could be explained to be due to the unevenness of the flaps being levelled as the upper platen starts to compress the carton (Kueh et al., 2019). Following this point is a linear region with the highest slope which gradually decreases up until the maximum load and is related to local buckling on the package (Kueh et al., 2019). Next, a sharp decrease in the maximum load occurs as the package fails (Viguié et al., 2010). Additionally, the results from the package compression showed that the Control package was stiffer than both the Standard vent and the Multi vent designs (Fig. 6). The observation is further corroborated in the compression strength (maximum force obtained at the end of the compression test of the package) of the packages as shown in Fig. 7a, with its corresponding displacements shown in Fig. 7b for all the package designs. From Fig. 7a, the compression strength of the unvented Control package was the highest, with an average value of 9176.50 N. When the compression strength of the Standard vent (7298.36 N) and Multi vent (5749.60 N) designs was compared with that of the Control package, a reduction in strength of approximately 20% and 37% was observed, respectively. Furthermore, there was a significant difference ($p < 0.05$) in the compression strength of all the package designs. These results show the crucial role of the ventilation openings on the package strength (Fadiji et al., 2019a; Dimitrov and Heydenrych, 2009). Besides, the lower compression strength

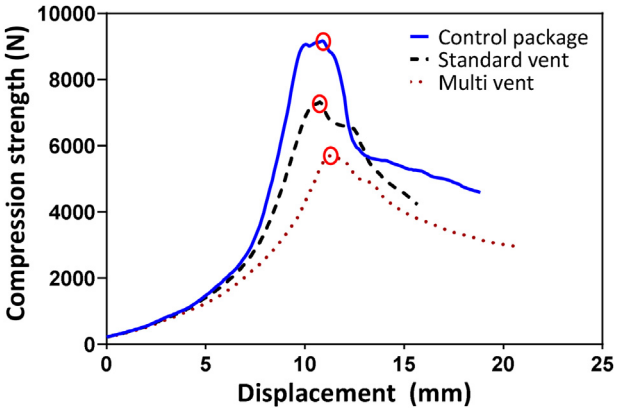

Fig. 6 – A typical load-displacement curve from the compression test for all the package designs. The circle in red in the figure indicates the maximum load. (For interpretation of the references to color in this figure legend, the reader is referred to the web version of this article.)

observed for the Multi vent design may be attributed to the number of vent holes. For instance, the Multi vent design has multiple smaller vent holes distributed along the lengthside of the package compared to the 3 vent holes of the Standard vent and the unvented Control package, which has no vent holes.

The average crosshead displacement obtained at the maximum compression strength for all the package designs is shown in Fig. 7b. Package displacement is a measure of the extent a package will be compressed at the end of a compression test. From Fig. 7b, the Multi vent design had the highest displacement of about 11.5 ± 0.2 mm, while the displacement of the Standard vent design and the Control package was approximately 10.3 ± 0.3 mm and 10.5 ± 0.2 mm, respectively. No significant difference ($p < 0.05$) in the displacement of the Control package and the Standard vent design was observed. However, the displacement obtained for the Multi vent design was significantly different ($p < 0.05$) from the displacement of the Control package and the Standard vent design. These findings showed that the geometrical configuration, for instance, vent holes of the packages have an effect on the displacement of the package under compression, hence indicating that the failure criterion for the packages in compression can be based on the displacement. In horticultural packaging, the maximum displacement where a package fails is important since it indicates whether the produce would be damaged or not if the

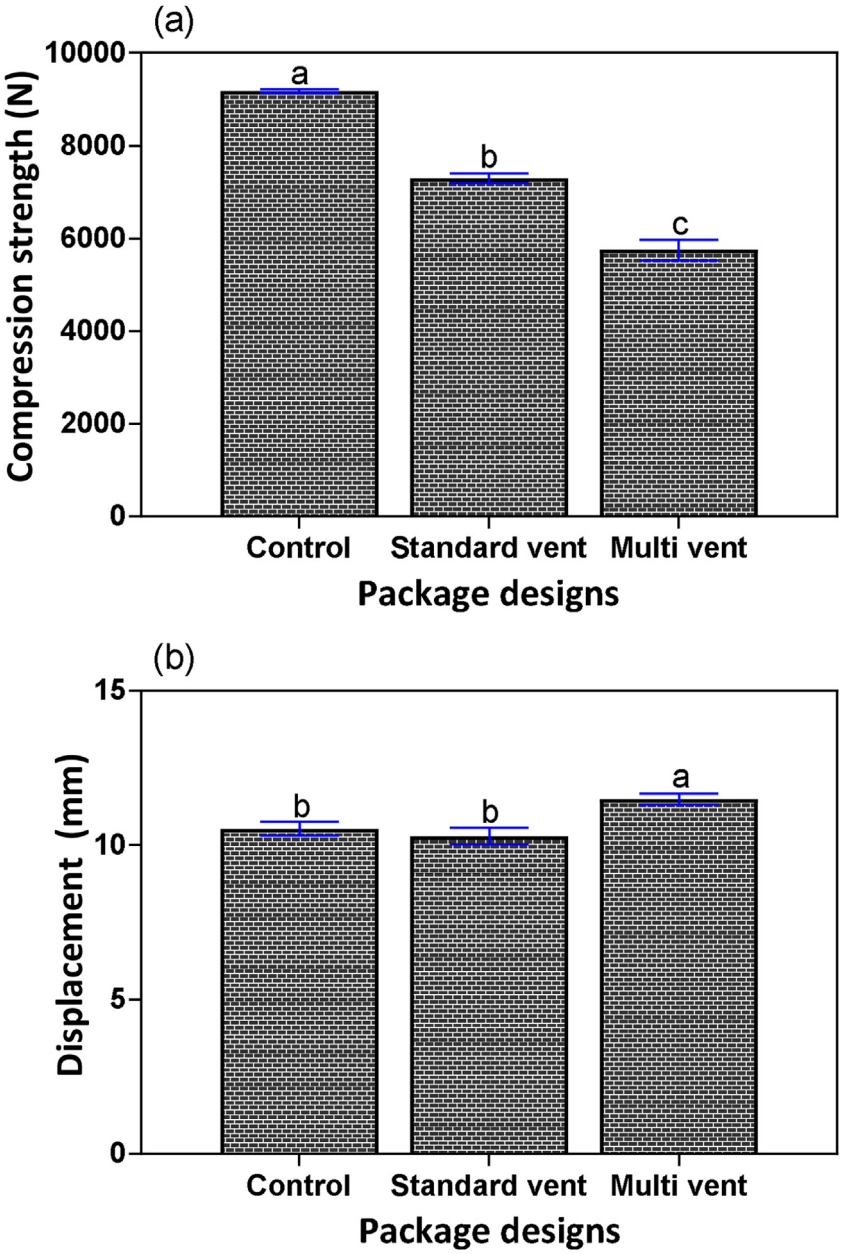

Fig. 7 – Bar chart showing (a) average compression strength (N) and (b) corresponding displacements for all the package designs. The letters on the error bars are used to show the statistical difference. Mean values with the same letters are not statistically different at $p < 0.05$.

package deforms but does not collapse completely (Defraeye et al., 2015).

4.2. *Evolution of the displacement field during compression*

Typically, the output from the 3D DIC is u, v and w displacement maps and the shape of the measured image, representing displacements in the x-, y- and z-directions (Fig. 3), respectively. It is worth mentioning that the displacement in the x- and y-directions are the in-plane displacements while the displacement in the z-direction is the out-of-plane displacement. A typical contour plots illustrating the displacement field in the out-of-plane direction (z-direction) for the reference image, taken before the compression test for all the package designs are shown in Fig. 8. Fig. 9 shows the displacement field in the three directions that occurred mid-way through the compression test while Fig. 10 shows the displacement field that occurred when the package reached its maximum force, i.e. the compression strength. From Fig. 8, the initial displacement before the start of the compression test, for all the package designs was approximately zero which increases during the test till failure. This was approximated on the plot to show exactly zero, however, the deviations from zero that was observed showed that the packages exhibited variations in the flatness of the panels, which may be due imperfections during manufacturing. Besides, this is also an indication of the predominance of panel buckling phenomenon even at the initiation of compression load.

Generally, during the compression of the packages, the displacement for all the package designs had a largely heterogeneous distribution as shown in the displacement fields. The fibre heterogeneity of paper material has been explained in detail in the study by De Oliveira et al. (1990) and will not be discussed in this study. As shown in the ROI, a clear distinction was observed in the displacement field behaviour mid-way

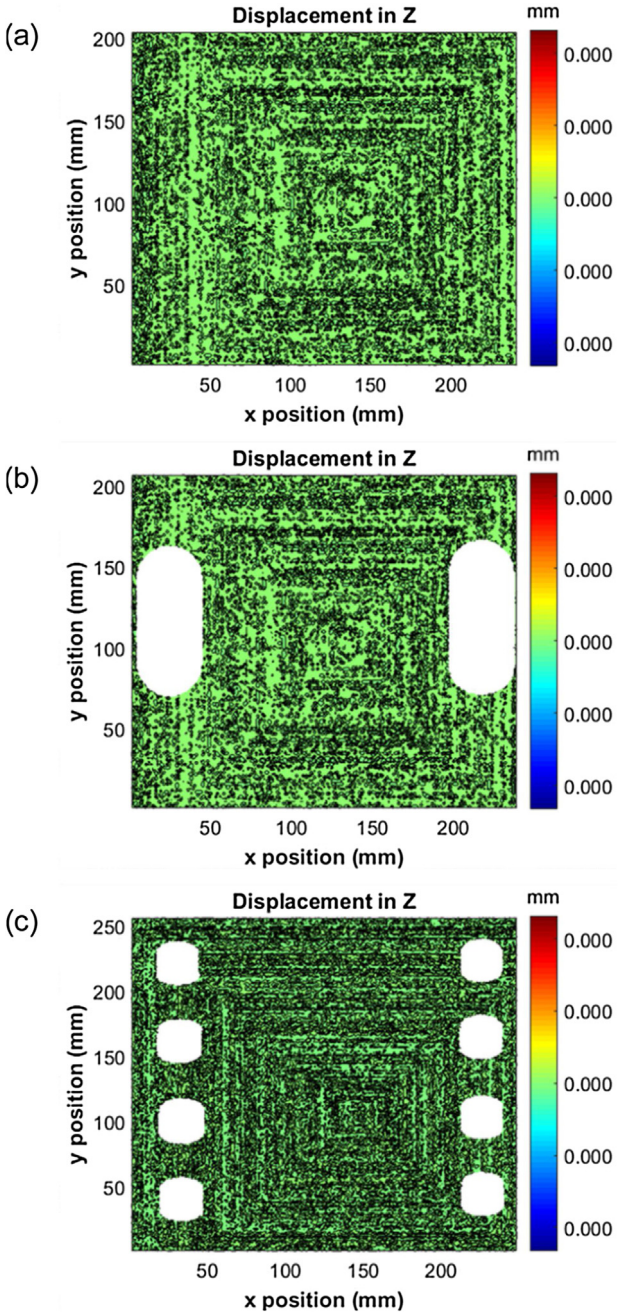

Fig. 8 – Typical out-of-plane (z-direction) displacement field of the reference image taken before the compression test for (a) control package, (b) standard vent and (c) multi vent.

through the compression test and at failure. The displacement field taken mid-way through the test (Fig. 9), was highly heterogeneous, and was observed to be influenced by the package design. The displacement in the x-direction was highest at the bottom of the ROI for the Control package while for the Standard vent and Multi vent packages, the displacement at the top of the package was highest. In the y-direction, the highest displacement was observed at the right edge of the ROI which gradually decreases towards the left edge of the ROI for all the package designs. The magnitude of the maximum displacement was approximately 5.8 mm, 5.3 mm and 6.8 mm for the Control package, Standard vent and Multi vent designs, respectively. Unlike the displacement fields in the x- and y-directions, the displacement field in the z-direction was highest at the top right corner for the Control package while for the Standard and Multi vent designs, the displacement was highest at the bottom left corner. Furthermore, the displacement in the x-, y- and z-direction mid-way through the compression test was observed to be of the same order. It is worth noting that the displacement in the y-direction was highest for all the package designs at this stage, and the direction was in the negative y-direction, indicating the effect of the compressive load.

Similarly, the displacement field of the maximum deformed image (at the end of the compression test) was also highly heterogeneous and was influenced by the package design (Fig. 10). Comparatively, for all the package designs, the displacement field in the x-direction was smaller than the displacement field in the y- and z-directions. Similar observations were reported in the study by Viguié et al. (2011). In addition, the displacement field in the x-direction for all the package designs behaved differently. For the Control package, the magnitude of the displacement in the x-direction at the top of the ROI was nearly zero, with the highest displacement located

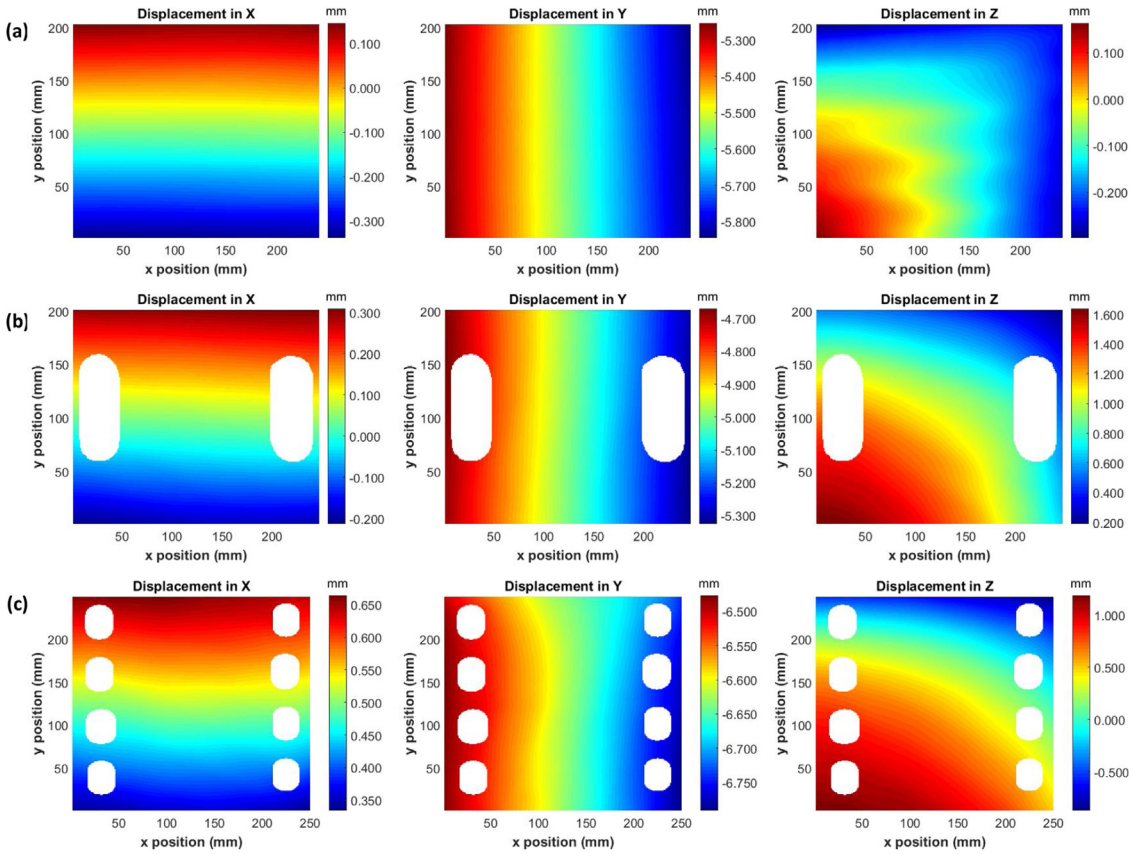

Fig. 9 – Displacement field of the image taken mid-way through the compression test for (a) control package, (b) standard vent and (c) multi vent.

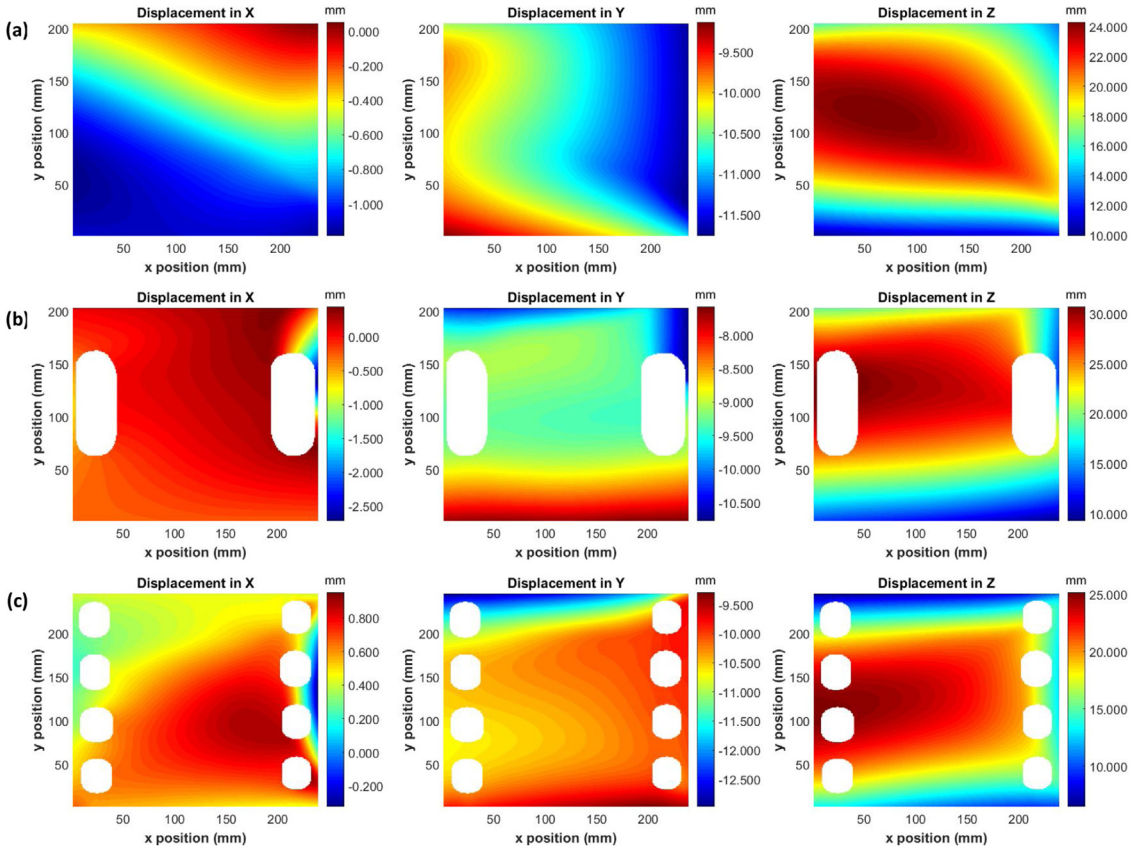

Fig. 10 – Displacement field of the maximum deformed image for (a) control package, (b) standard vent and (c) multi vent.

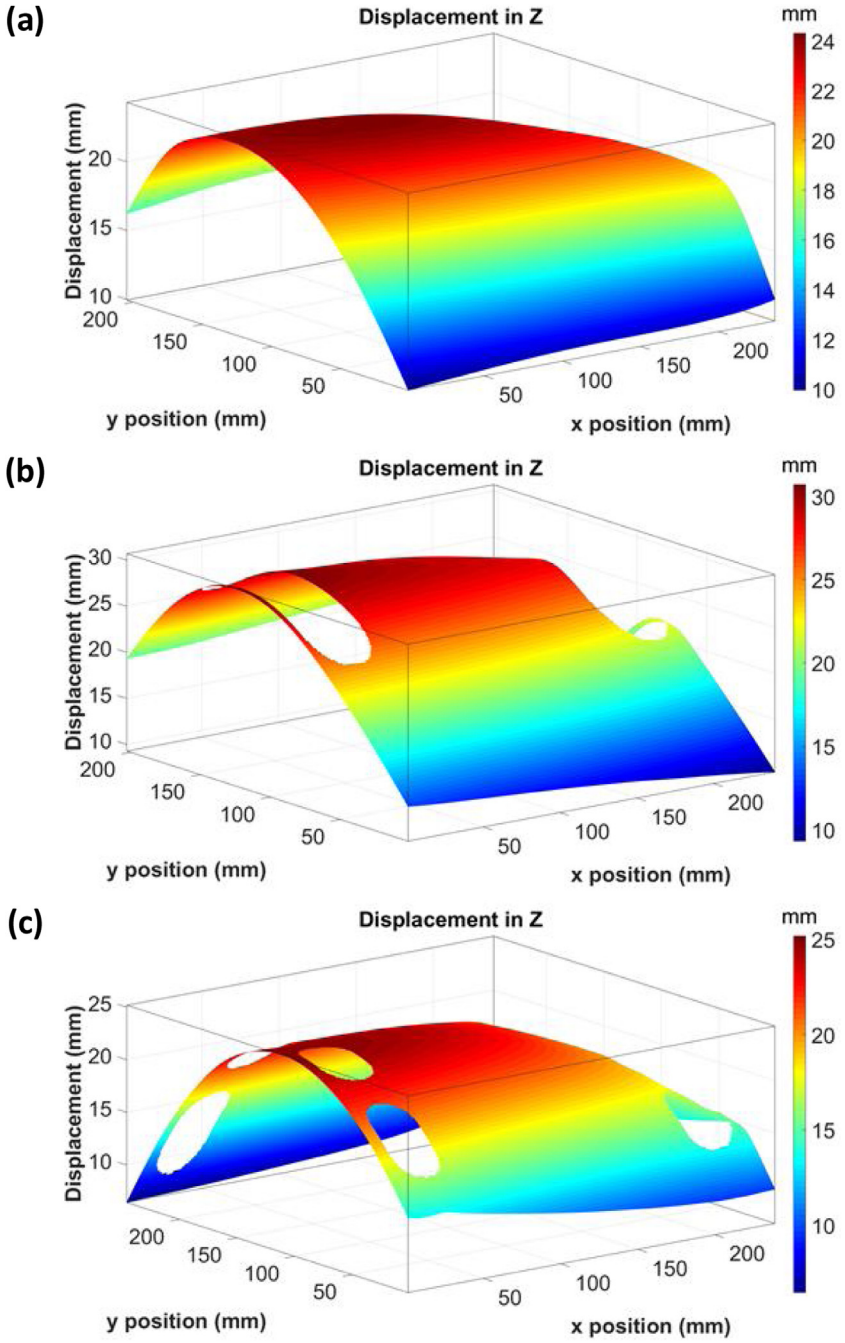

Fig. 11 – The out-of-plane displacement field of the maximum deformed image showing the buckling shape for (a) control package, (b) standard vent and (c) multi vent.

towards the bottom of the ROI and mostly negative. Highest displacement was located at the right edges of the ROI and around the vent for the Standard vent, with the displacement at the surface being homogenous and approximately zero. For the Multi vent, the displacement in the x-direction was highest towards the centre of the ROI. Also, the displacement in the y-direction was observed to be nearly homogenous over the surface of the ROI for all the package designs. Furthermore, the displacement in the y-direction was negative, indicating the downward movement of the panel as a result of the compressive load. Maximum displacement in the y-direction was mostly located at the top of the ROI of the package panels. This can be attributed to the vertical translatory movement exhibited during the box compression test (BCT). Additionally, this may also be due to the crushing that occurs at the junction score of the package during the BCT. The magnitude of the maximum displacement for the Control package, Standard vent and Multi vent designs was approximately 11.5 mm, 10.5 mm and 12.5 mm, respectively. The displacement in the z-direction i.e. the out-of-plane displacement was highest and was located towards the centre of the package panels, which decreases towards the edges of the ROI. This indicated the predominance of buckling at the centre of the package panels.

The distribution of the out-of-plane displacement field for all the package designs was in the range of about 10–30 mm. The magnitude of the maximum out-of-plane displacement for the Control package, Standard vent and Multi vent designs was approximately 24 mm, 30 mm and 25 mm, respectively. The buckling shape of the out-of-plane displacement field for all the packages is shown in Fig. 11. From Fig. 11, there was an outward buckling of the package panel of the deformed image, concentrated near the middle of the panel. This was

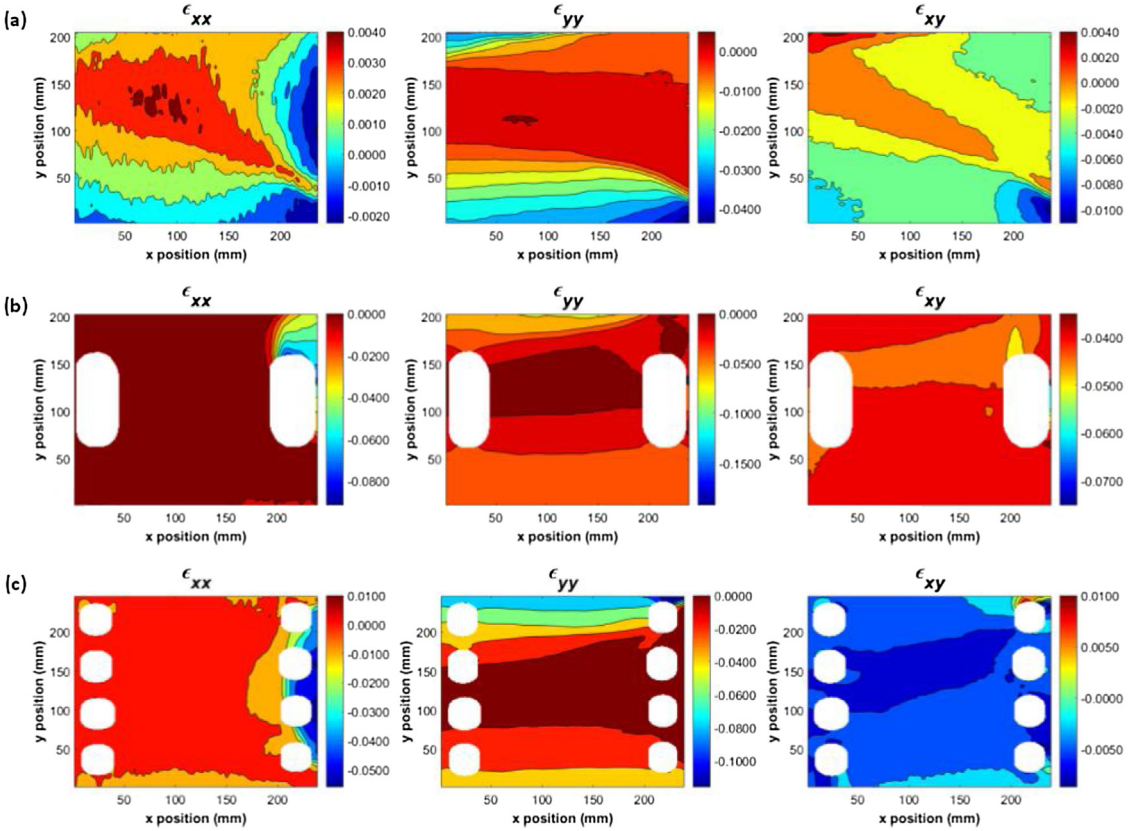

Fig. 12 – Strain field components of the maximum deformed image for (a) control package, (b) standard vent and (c) multi vent.

also observed to start with small initial outward displacements which increases gradually during the BCT as shown in Figs. 8 and 9. Similar observations were reported by Kueh et al. (2019). During stacking on a pallet, the packages placed at the bottom of the stack tend to experience the highest loads resulting in a significant out-of-plane deformation of the vertical walls before total collapse (Viguié et al., 2011). In addition, the out-of-plane displacement is usually small when the load level is below the maximum strength of the package (Fig. 9), however, on reaching the maximum load, the package deforms rapidly hence decreasing the in-plane stiffness and increasing the out-of-plane displacement as can be seen in Fig. 10 (Allansson and Svärd, 2001). This results also indicated that carton geometry and the vent hole designs predispose compression towards a certain failure pattern.

The components ε_{xx}, ε_{yy} and ε_{xy} of the strain field for the deformed image are shown in Fig. 12. The strain behaviour for all the components was different for all the package designs. This shows that the deformation mechanisms can be significantly affected by the configuration of the package. However, it was observed that the variation in strain was more prominent along the edges of the ROI. Contrary to this observation, strain values were approximately zero for most of the components of the strain field at the centre of the ROI. The strain variation for the ε_{xx} component was more pronounced along the vertical edges of the ROI while that of the ε_{yy} component was more pronounced along the horizontal edges of the ROI, and was mostly compressive. It is interesting to mention that the strain was more localised in the ε_{xx} component for the Standard and Multi vent design, particularly around the vent holes. Meanwhile in the Control package, high intensity of the ε_{xx} component was observed compared to Standard and Multi vent packages. Similar observation was reported by Viguié et al. (2011) for carton without vent holes. This reveals the complexity of the deformation mechanism of paperboard package and its dependence of geometrical configurations. Additionally, the negative values shown in the strain components is an attribute of a compressive deformation state. The characterisation of the mechanical heterogeneity of paperboard packages will help provide package designers with relevant information for control during manufacturing.

5. Conclusions

The DIC technique is a full-field non-contact optical technique for measuring displacements in experimental testing. A 3D DIC technique was applied to measure the full-field displacement and strain at the surface of three corrugated paperboard packages during compression loading. The packages used were unvented Control package and two VCP packages (Standard and the Multi vent). The Control package had the greatest compression strength while the Multi vent package had the lowest compression strength. The results showed the development and behaviour of buckling on the surface of the package. The displacements of the packages were observed to be largely heterogeneous in its distribution. The displacement field in the *x*-direction was smaller compared to that in the *y*- and *z*-direction. Furthermore, for the maximum deformed image, the out-of-plane displacement (i.e. *z*-direction) had the highest displacement values, with maximum value of approximately 24 mm for the Control package, 30 mm for the Standard vent and 25 mm for the Multi vent. In addition, the displacement was highest in the *z*-direction at the centre of the ROI and an outward buckling was observed for all the package designs. Package designs affected the strain variation, although strain values were approximately zero at the centre

of the ROI. The strain components ε_{xx} and ε_{yy} were observed to be more prominent along the vertical and horizontal edges respectively irrespective of the package design. A significant finding in this study is the dependency of the displacement and strain variation on package design. Additionally, this work contributes and provides preliminary evidence of the potential use of DIC to understanding the failure mechanisms of ventilated packages under compression load, offering prospects for enhancing the overall packaging performance through the design of vents that will maintain a balance between the mechanical integrity of the package and uniform air distribution within the package system. Future study will incorporate quantifying the interaction of the package with its content, and the effect on the displacement field of the package. Furthermore, the influence of the aspect ratio, size, dimensions, and distortions in shape of the vent holes and package on the mechanical behaviour of the package during compression as well as wider ROI close to the corner of the package will be included in future studies.

Competing interests

None.

Acknowledgments

This work is based on the research supported wholly by the National Research Foundation of South Africa (Grant Number: 64813). The financial support of the National Research Foundation of South Africa through the award of postdoctoral fellowship to Dr Fadiji is gratefully acknowledged (IUD: 120797). The opinions, findings and conclusions or recommendations expressed are those of the authors alone, and the NRF accepts no liability whatsoever in this regard. The packages were obtained from APL Cartons, Worcester, South Africa and the authors appreciate the staff for their support.

References

Allansson, A., Svärd, B., 2001. Stability and Collapse of Corrugated Board; Numerical and Experimental Analysis. Lund University (Master's Thesis).

ASTM, 2006. D4332-01: Standard Practice for Conditioning Containers, Packages, or Packaging Components for Testing. American Society of Testing and Materials International, West Conshohocken, PA.

ASTM, 2010. ASTM D642: Standard Test Method for Determining Compressive Resistance of Shipping Containers, Components, and Unit Loads. American Society of Testing and Materials International, West Conshohocken, PA.

Berry, T.M., Fadiji, T.S., Defraeye, T., Opara, U.L., 2017. The role of horticultural carton vent hole design on cooling efficiency and compression strength: a multi-parameter approach. Postharvest Biol. Technol. 124, 62–74.

Chasiotis, I., Knauss, W.G., 2002. A new micro-tensile tester for the study of MEMS materials with the aid of atomic force microscopy. Exp. Mech. 42 (1), 51–57.

Considine, J.M., Scott, C.T., Gleisner, R., Zhu, J.Y., 2005. Use of digital image correlation to study the local deformation field of paper and paperboard. 13th Fundamental Research Symposium Conference, September, 613–630.

De Oliveira, R.C., Mark, R.E., Perkins, R.W., 1990. Evaluation of the effects of heterogeneous structure on strain distribution in low density papers. Mech. Wood Paper Mater. 112, 37–61.

Defraeye, T., Cronjé, P., Berry, T., Opara, U.L., East, A., Hertog, M., Verboven, P., Nicolai, B., 2015. Towards integrated performance evaluation of future packaging for fresh produce in the cold chain. Trends Food Sci. Technol. 44, 201–225.

Dimitrov, K., Heydenrych, M., 2009. Relationship between the edgewise compression strength of corrugated board and the compression strength of liner and fluting medium papers. Southern Forests 71 (3), 227–233.

Fadiji, T., Coetzee, C., Chen, L., Chukwu, O., Opara, U.L., 2016a. Susceptibility of apples to bruising inside ventilated corrugated paperboard packages during simulated transport damage. Postharvest Biol. Technol. 118, 111–119.

Fadiji, T., Coetzee, C., Opara, U.L., 2016b. Compression strength of ventilated corrugated paperboard packages: numerical modelling, experimental validation and effects of vent geometric design. Biosyst. Eng. 151, 231–247.

Fadiji, T., Coetzee, C.J., Berry, T.M., Ambaw, A., Opara, U.L., 2018. The efficacy of finite element analysis (FEA) as a design tool for food packaging: a review. Biosyst. Eng. 174, 20–40.

Fadiji, T., Coetzee, C.J., Berry, T.M., Opara, U.L., 2019a. Investigating the role of geometrical configurations of ventilated fresh produce packaging to improve the mechanical strength – experimental and numerical approaches. Food Packag. Shelf Life 20, 100312.

Fadiji, T., Coetzee, C.J., Opara, U.L., 2019b. Analysis of the creep behaviour of ventilated corrugated paperboard packaging for handling fresh produce – an experimental study. Food Bioprod. Process. 117, 126–137.

Flatscher, T., Daxner, T., Pahr, D.H., Rammerstorfer, F.G., 2011. Optimization of corrugated paperboard under local and global buckling constraints. Multisc. Methods Comput. Mech. 55, 329–346.

Godara, A., Raabe, D., Bergmann, I., Putz, R., Müller, U., 2009. Influence of additives on the global mechanical behaviour and the microscopic strain localization in wood reinforced polypropylene composites during tensile deformation investigated using digital image correlation. Compos. Sci. Technol. 69 (2), 139–146.

Gong, G., Liu, Y., Fan, B., Sun, D., 2020. Deformation and compressive strength of corrugated cartons under different indentation shapes: experimental and simulation study. Packag. Technol. Sci. 33 (6), 215–226.

Huchzermeyer, R.L., 2017. Measuring Mechanical Properties Using Digital Image Correlation: Extracting Tensile and Fracture Properties from a Single Sample. Stellenbosch University (Masters Thesis).

Hung, P.C., Voloshin, A.S., 2003. In-plane strain measurement by digital image correlation. J. Braz. Soc. Mech. Sci. Eng. 25 (3), 215–221.

Kolanu, N.R., Prakash, S.S., Ramji, M., 2016. Experimental study on compressive behavior of GFRP stiffened panels using digital image correlation. Ocean Eng. 114, 290–302.

Kueh, C.S., Dahm, K., Emms, G., Wade, K., Bronlund, J.E., 2019. Digital image correlation analysis of vertical strain for corrugated fiberboard box panel in compression. Packag. Technol. Sci. 32 (3), 133–141.

Pan, B., 2018. Digital image correlation for surface deformation measurement: historical developments, recent advances and future goals. Meas. Sci. Technol. 29 (8), 082001.

Pan, B., Li, K., 2011. A fast digital image correlation method for deformation measurement. Opt. Lasers Eng. 49 (7), 841–847.

Pan, B., Qian, K., Xie, H., Asundi, A., 2009. Two-dimensional digital image correlation for in-plane displacement and strain measurement: a review. Meas. Sci. Technol. 20 (6), 062001.

Pan, B., Xie, H., Wang, Z., 2010. Equivalence of digital image correlation criteria for pattern matching. Appl. Opt. 49 (28), 5501–5509.

Pan, B., Wu, D., Xia, Y., 2012. An active imaging digital image correlation method for deformation measurement insensitive to ambient light. Opt. Laser Technol. 44 (1), 204–209.

Pathare, P.B., Opara, U.L., 2014. Structural design of corrugated boxes for horticultural produce: a review. Biosyst. Eng. 125, 128–140.

Tang, Z., Liang, J., Xiao, Z., Guo, C., 2012. Large deformation measurement scheme for 3D digital image correlation method. Opt. Lasers Eng. 50 (2), 122–130.

Tekieli, M., De Santis, S., de Felice, G., Kwiecień, A., Roscini, F., 2017. Application of digital image correlation to composite reinforcements testing. Compos. Struct. 160, 670–688.

Thorpe, J.L., Choi, D., 1992. Corrugated container failure part 2 – strain measurements in laboratory compression tests. Tappi J. 75 (7), 155–161.

Viguié, J., Dumont, P.J.J., 2013. Analytical post-buckling model of corrugated board panels using digital image correlation measurements. Compos. Struct. 101, 243–254.

Viguié, J., Dumont, P.J., Desloges, I., Mauret, É., 2010. Some experimental aspects of the compression behaviour of boxes made up of G-flute corrugated boards. Packag. Technol. Sci. 23 (2), 69–89.

Viguié, J., Dumont, P.J.J., Orgéas, L., Vacher, P., Desloges, I., Mauret, E., 2011. Surface stress and strain fields on compressed panels of corrugated board boxes. An experimental analysis by using Digital Image Stereocorrelation. Compos. Struct. 93 (11), 2861–2873.

Wong, L., Kortschot, M.T., Dodson, C.T.J., 1996. Effect of formation on local strain fields and fracture of paper. J. Pulp Paper Sci. 22 (6), J213–J219.

Zhou, J.W., Liu, D.H., Shao, L.Y., Wang, Z.L., 2013. Application of digital image correlation to measurement of packaging material mechanical properties. Math. Probl. Eng.